Electrically tuned Förster resonances in collisions of NH_3 with Rydberg He atoms

V. Zhelyazkova and S. D. Hogan
Department of Physics and Astronomy, University College London, Gower Street, London WC1E 6BT, United Kingdom

(Received 3 November 2016; published 21 April 2017)

The effects of weak electric fields on resonant energy transfer between NH_3 in the $X\ ^1A_1$ ground electronic state and Rydberg He atoms in triplet states with principal quantum numbers $n = 36$–41 have been studied in a crossed-beam apparatus. For these values of n, electric dipole transitions between the Rydberg states that evolve adiabatically to the $|ns\rangle$ and $|np\rangle$ states in zero electric field can be tuned into resonance with the ground-state inversion transitions in NH_3 using electric fields, with energy transfer occurring via Förster resonance. In the experiments the Rydberg He atoms, traveling in pulsed supersonic beams, were prepared by resonant two-photon excitation from the metastable $1s2s\ ^3S_1$ level and crossed an effusive beam of NH_3 before being detected by state-selective pulsed-electric-field ionization. The resonant-energy-transfer process was identified by monitoring changes in the ionization signal from the $|ns\rangle$ and $|np\rangle$ Rydberg states for each value of n. The electric-field dependence of the experimental data is in good agreement with the results of calculations in which the resonant dipole-dipole coupling between the collision partners was accounted for.

DOI: 10.1103/PhysRevA.95.042710

I. INTRODUCTION

Energy transfer between quantum systems coupled by resonant electric dipole interactions plays an important role in inter- and intramolecular dynamics, particularly in excited electronic states [1,2]. These Förster resonance processes [3–5] are, for example, exploited in single-molecule spectroscopy [6] and contribute to excitation transfer in light-harvesting complexes [7]. The electric dipole-dipole coupling $V_{\rm dd}$ that gives rise to such energy transfer between two systems, A and B, has the form [8]

$$V_{\rm dd}(\vec{R}) = \frac{1}{4\pi\epsilon_0}\left[\frac{\vec{\mu}_A\cdot\vec{\mu}_B}{R^3} - 3\frac{(\vec{\mu}_A\cdot\vec{R})(\vec{\mu}_B\cdot\vec{R})}{R^5}\right], \quad (1)$$

where $\vec{\mu}_A = \langle f_A|\hat{\vec{\mu}}_A|i_A\rangle$ and $\vec{\mu}_{\rm B} = \langle f_B|\hat{\vec{\mu}}_B|i_B\rangle$ are the electric dipole transition moments between the initial, i, and final, f, internal quantum states of A and B, respectively, and $R = |\vec{R}|$ is the distance between the systems. The angular dependence of the scalar products in Eq. (1) reflects the sensitivity of the energy-transfer process to the orientation of the dipoles and hence the characteristics of their local environment. Consequently, $V_{\rm dd}$ and the rates of energy transfer can be strongly modified by static, or time-dependent, electric and magnetic fields.

Because of (i) the large electric dipole moments of transitions between Rydberg states with a high principal quantum number n, e.g., $|\langle np|\hat{\vec{\mu}}|ns\rangle| \geqslant 1000ea_0$ for $n \geqslant 36$ in He, (ii) the tunability of Rydberg-Rydberg transition wave numbers using electric or magnetic fields, and (iii) the control over the environment that can be achieved in gas-phase experiments, Rydberg atoms have been successfully exploited as model systems with which to study Förster resonance energy transfer [8–12]. For example, resonant interactions between pairs of neutral atoms of a single species have been used to blockade laser photoexcitation [13] and generate pairwise entanglement [14], realize strong optical nonlinearities in cold atomic gases [15] to demonstrate single-photon optical transistors [16,17], and investigate energy transfer within tailored arrangements of atoms [18,19].

In addition to studies of resonant energy transfer between atoms in Rydberg states, experiments have also been reported in which resonant depopulation and ionization of Rydberg atoms in collisions with polar molecules were observed in the absence of external fields [20–23]. More recently, in the context of the development of methods for the preparation of ultracold polar molecules it has been proposed that resonant interactions with cold Rydberg gases could be exploited to cool the molecules [24,25]. To implement schemes of this kind it is essential to perform Rydberg-state-resolved studies of Förster resonances in these hybrid atom-molecule systems to identify and characterize the effects of external fields on these interactions. From a more general perspective, such measurements also offer new opportunities for investigations of the role of coherences between electronic, vibrational, and rotational degrees of freedom (see, e.g., Refs. [26,27] and references therein) and environmental effects in molecular resonance energy transfer, and studies of chemical dynamics in which long-range dipolar interactions can be exploited to regulate access to short-range Penning ionization processes [28] at low temperature.

In this paper we report the results of experiments in which we observe Förster resonance energy transfer from the inversion sublevels of the $X\ ^1A_1$ ground electronic state of NH_3 to He atoms in selected triplet Rydberg states with values of n from 36 to 41. Using electric fields up to 12 V cm^{-1}, electric-dipole transitions between the states that evolve adiabatically to the $|ns\rangle$ and $|np\rangle$ Rydberg states in zero electric field were tuned through resonance with the NH_3 inversion spectrum, modifying the energy-transfer rates. The interpretation of the experimental data is aided by comparison with the results of calculations of the electric-field dependence of the energy-transfer process.

II. EXPERIMENT

An overview of the experimental apparatus is presented in Fig. 1(a). Helium atoms traveling in pulsed supersonic beams (mean longitudinal speed 2000 m s^{-1}) were prepared in the metastable $1s2s\ ^3S_1$ level in a dc electric discharge at the exit

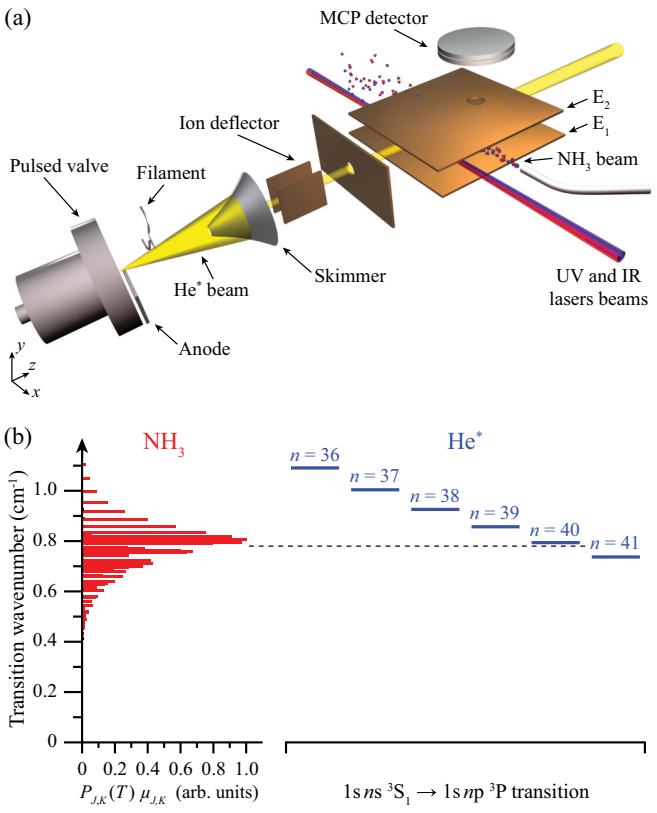

FIG. 1. (a) Schematic diagram of the experimental apparatus (not to scale). (b) Comparison of the transition-dipole-moment-weighted ground-state inversion spectrum of NH_3 at 300 K with the field-free wave numbers of $1sns\ ^3S_1 \rightarrow 1snp\ ^3P_J$ transitions in He.

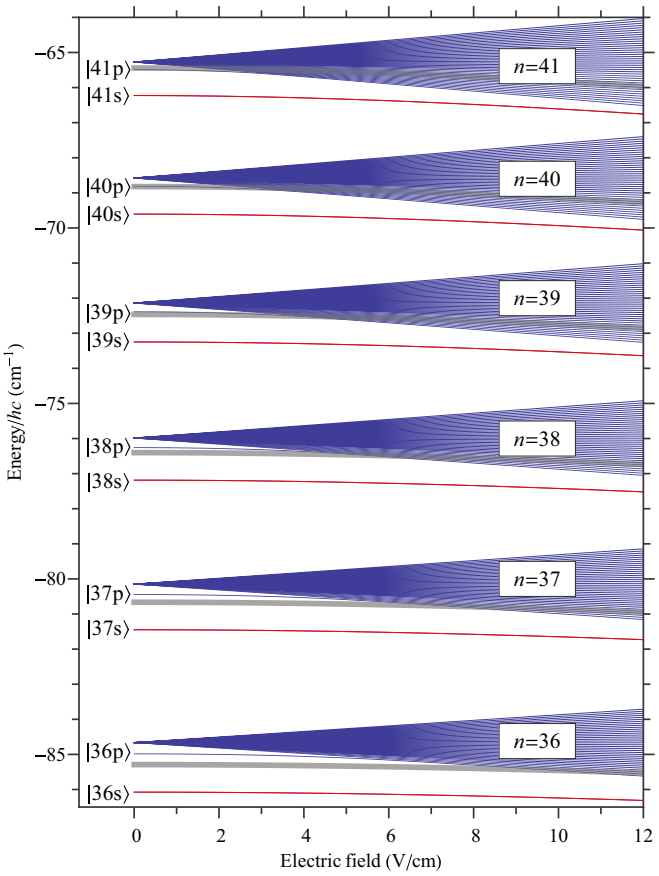

FIG. 2. Energy-level structure of the $m_\ell = 0$ triplet Rydberg states in He with $n = 36$–41. The $|ns\rangle$ levels photoexcited in the experiments are indicated in red. The gray shaded curves show the wave numbers of each $|ns'\rangle$ level offset by the centroid inversion wave number in NH_3 ($\sim$0.78 cm^{-1}).

of a pulsed valve [29]. After collimation and deflection of stray ions, the He beam was intersected by UV and IR laser radiation between two parallel 70 mm × 70 mm copper electrodes, E_1 and E_2 in Fig. 1(a), separated by 8.4 mm. The UV laser was frequency stabilized to drive the $1s2s\ ^3S_1 \rightarrow 1s3p\ ^3P_2$ transition at 25 708.588 cm^{-1} (≡388.975 nm). The IR laser was tuned in the range from 12 660 to 12 681 cm^{-1} (≡789.89 to 788.58 nm) to subsequently excite $1sns\ ^3S_1$ levels with $n = 36$–41. After photoexcitation, the typical number density of excited Rydberg atoms was $\sim 10^8$ cm^{-3} [30].

Rydberg state photoexcitation was performed in zero electric field for 3 μs. After this time, the field was switched (rise time of 200 ns) to a selected value, $F_{\rm int}$, by applying appropriate potentials to E_2, as the Rydberg atoms crossed an effusive beam of NH_3 emanating from a 1-mm-diameter tube maintained at 1.8 mbar and 300 K (mean speed of $\sim$720 m s^{-1}; number density of $\sim 2 \times 10^9$ cm^{-3} [31]). After an interaction time of 5 μs, $F_{\rm int}$ was switched back to zero before the Rydberg atoms were detected by ramped electric-field ionization upon applying pulsed potentials of up to $V_{\rm ion} \simeq -300$ V, rising with an RC time constant of 1.0 μs, to E_1. The ionized electrons were accelerated through a 4-mm-diameter hole in E_2 to a microchannel plate (MCP) detector. In this process, the Rydberg atoms in the center of the excited ensemble spent approximately equal periods of time (5 μs) in the interaction field $F_{\rm int}$ and in zero electric field.

III. EXPERIMENTAL RESULTS

The $|ns\rangle$ and $|np\rangle$ triplet Rydberg states in He (referring to the $1sns\ ^3S_1$ and $1snp\ ^3P_J$ levels in zero field, respectively) are separated by 0.73–1.1 cm^{-1} for $n = 36$–41, while the inversion transitions in the $X\ ^1A_1$ state of NH_3 lie at $\sim 0.78 \pm 0.2$ cm^{-1} at 300 K. The $|ns\rangle \rightarrow |np\rangle$ transition is therefore resonant with the NH_3 inversion spectrum at $n \simeq 40$ [see Fig. 1(b)]. The energy-level structure of the $m_\ell = 0$ triplet Rydberg states of He is displayed in Fig. 2 for electric fields up to 12 V cm^{-1}. Because of their nonzero quantum defects, e.g., $\delta_{36s} = 0.29669$ and $\delta_{36p} = 0.06835$ [32], the $|ns\rangle$ and $|np\rangle$ states at each value of n lie lower in energy in zero field than the higher-angular-momentum states. In increasing fields, the wave-number intervals between these two states reduce as they evolve into the $|ns'\rangle$ and $|np'\rangle$ ℓ-mixed Stark states. The gray shaded curves in Fig. 2, shifted in wave number from each $|ns'\rangle$ state by the centroid NH_3 inversion wave number ($\sim$0.78 cm^{-1}), show that electric fields in the range encompassed in the figure can be used to tune the two systems through resonance.

Because the $|ns\rangle$ and $|np\rangle$ Rydberg states ionize in different electric fields, energy transfer in collisions with NH_3 can be identified from the electron time-of-flight profiles in the time-dependent ionization fields. The slight asymmetry in this

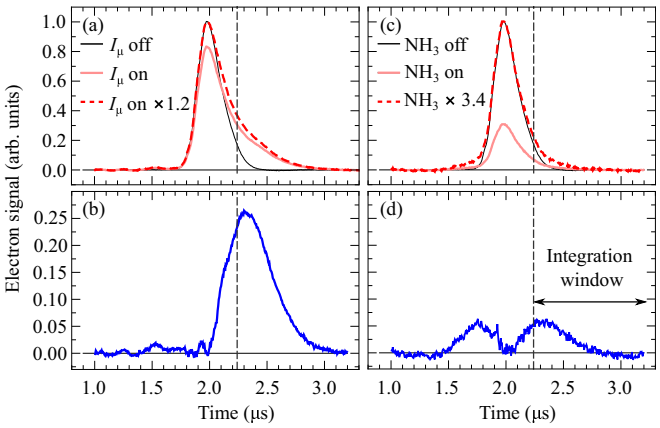

FIG. 3. Electric-field ionization profiles at $n = 38$ in He demonstrating (a) and (b) the effect of microwave transfer of population from the $|38s\rangle$ state to the $|38p\rangle$ state and (c) and (d) collisions with NH_3. In (a) and (c) the unperturbed $|38s\rangle$ signal is indicated by the thin black curve, and the un-normalized (normalized) profiles recorded following microwave transfer or collisions are indicated by the thick pink (dashed red) curves. The dashed vertical line in each panel marks the start of the integration window used to identify the $|np\rangle$ signal in Fig. 4.

profile results from the transient response of the *RC* charging circuit used to generate the ramped ionization electric field. An example of such a ramped field ionization profile for the $|38s\rangle$ state is displayed in Fig. 3(a) (thin black curve). To identify changes in this profile when the $|38p\rangle$ state is populated, a reference measurement was made in which population was transferred to the $|38p\rangle$ state with $|m_\ell| = 1$ by a pulse of microwave radiation with no NH_3 present [thick pink curve in Fig. 3(a)]. Following normalization of these data recorded with the microwaves on [dashed red curve in Fig. 3(a)] and subtraction of the profile for the $|38s\rangle$ state alone, the contribution from the $|38p\rangle$ state to the signal is seen [Fig. 3(b)]. In the time-dependent ionization fields used in the experiments the $|np\rangle$ states with $|m_\ell| = 1$ ionize quasidiabatically and therefore at higher fields than the $|ns\rangle$ states, which ionize adiabatically. The $|np\rangle$ states with $m_\ell = 0$ also ionize adiabatically, but in fields slightly lower than those of the $|ns\rangle$ states because of their smaller quantum defects. Consequently, complete $|m_\ell|$-state selective detection was achieved.

Using this $|38p\rangle$ signal as a guide, the effects of collisions with the beam of NH_3 in the absence of the microwaves were determined. The ionization profile of the $|38s\rangle$ state with $F_{\rm int} = 0.6$ V cm^{-1} and NH_3 present is displayed in Fig. 3(c) (thick pink curve). The total electron signal is significantly reduced following collisions with NH_3 as a result of n changing associated with rotational energy transfer, and collisional ionization [22]. When normalized to the intensity maximum of the pure $|38s\rangle$ signal, the state-changing effects of the collisions can be seen, with some population detected in the ionization time window associated with the $|38p\rangle$ state. Similar profiles for $n = 36$–41 all displayed population of the $|np\rangle$ state at ionization times beyond 2.24 μs when $V_{\rm ion}$ was set so that the $|ns\rangle$-electron signal was detected at the same time of flight for each value of n. After the time window corresponding to the ionization of atoms in the $|np\rangle$

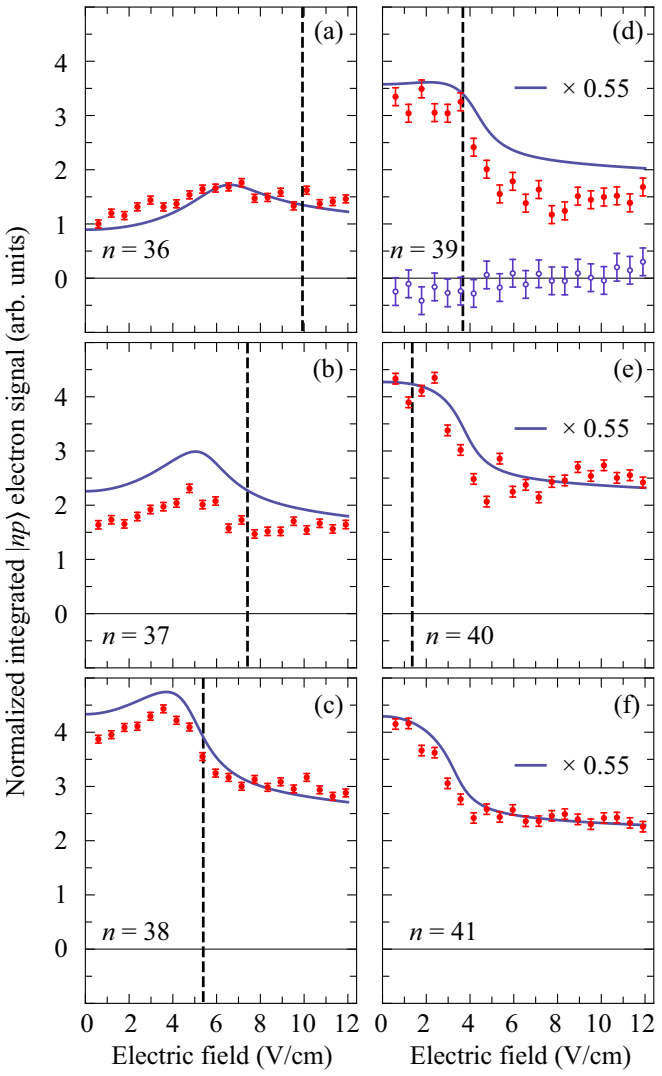

FIG. 4. (a)–(f) Integrated $|np\rangle$ electron signal recorded following collisions of NH_3 with He atoms prepared in $|ns\rangle$ states with $n = 36$–41. All data sets are normalized relative to the first data point in (a). The dashed vertical lines indicate the electric field at each value of n for which the centroid inversion splitting in NH_3 is resonant with the $|ns'\rangle \rightarrow |np'\rangle$ transition in He. The solid curves represent the normalized dependence of the calculated $|np\rangle$-electron signal in the electric field. In (d)–(f) the results of the calculations are scaled by a factor of 0.55. A reference measurement with the NH_3 beam replaced with a beam of NO is indicated by the open circles in (d).

states was identified, the effects of the electric fields on the energy-transfer process were investigated. This was done by integrating the electron signal in the $|np\rangle$ detection window [see Fig. 3(d)] for $F_{\rm int} = 0.6$ –12 V cm^{-1}, with the results displayed in Fig. 4.

For the lower values of n [e.g., $n = 36$–38 in Figs. 4(a)–4(c)] the zero-field $|ns\rangle \rightarrow |np\rangle$ transition lies above the centroid transition wave number of the NH_3 inversion spectrum [see Fig. 1(b)]. When $F_{\rm int}$ is increased, the reduction in the wave-number interval between the $|ns'\rangle$ and $|np'\rangle$ states brings the energy-transfer channel into resonance and causes an increase in the $|np\rangle$-electron signal observed up to $F_{\rm int} \simeq 7, 5,$

and 4 V cm^{-1} in Figs. 4(a), 4(b), and 4(c), respectively. For values of n between 39 and 41 [Figs. 4(d)–4(f)], there is sufficient overlap between the zero-field $|ns\rangle \rightarrow |np\rangle$ transition wave number and the inversion spectrum for resonance energy transfer to occur even in the weakest fields investigated. In these measurements and in fields exceeding 8 V cm^{-1} for $n < 39$, the $|np\rangle$-electron signal reduces as $F_{\rm int}$ is increased. This reflects the shift away from resonance of the energy-transfer process.

To confirm the origin of the resonance features in the data in Fig. 4, the NH_3 beam was replaced with an effusive beam of NO emanating from the same source. Since there are no electric-dipole transitions in the $X\ ^2\Pi$ ground state of NO in the spectral region close to 1 cm^{-1}, no resonant transfer to the $|np\rangle$ state is expected for the fields in Fig. 4. This is confirmed in the data recorded at $n = 39$ and presented in Fig. 4(d) (open circles).

IV. CALCULATIONS

To obtain further insight into the Förster resonance energy-transfer process and the dependence of the experimental data in Fig. 4 on $F_{\rm int}$, energy-transfer cross sections were calculated following the approach employed to treat collisions between pairs of Rydberg atoms in Ref. [8]. These calculated cross sections were used to determine the resonance widths and, when combined with the Stark shifts of the $|ns'\rangle$ and $|np'\rangle$ Rydberg states, the dependence of the $|np\rangle$-electron signal on $F_{\rm int}$.

For a constant collision speed, the cross section for resonant energy transfer $\sigma_{J,K}(F_{\rm int})$ from each rotational state $|J,K\rangle$ in NH_3, where J is the total angular momentum quantum number and K is the projection of $\vec{J}$ onto the symmetry axis of the molecule, to a He Rydberg atom is

$$\sigma_{J,K}(F_{\rm int}) \propto \mu_{ns',np'}(F_{\rm int})\,\mu_{J,K}, \tag{2}$$

where $\mu_{ns',np'}(F_{\rm int}) = |\langle np'|\hat{\vec{\mu}}|ns'\rangle|$ is the electric dipole transition moment between the $|ns'\rangle$ and $|np'\rangle$ states and

$$\mu_{J,K} = \sqrt{\frac{\mu_0^2\,K^2}{J(J+1)}} \tag{3}$$

is the transition dipole moment associated with the inversion of the NH_3 molecule in the $|J,K\rangle$ state, with $\mu_0 = 1.468$ D [33]. The Rydberg-Rydberg transition dipole moments were calculated from the eigenvectors of the Hamiltonian matrix describing the interaction of the He atom with the electric field [34]. In the experiments the NH_3 molecules were not aligned or oriented. To account for this in the calculations, $V_{\rm dd}$ in Eq. (1) was averaged over all angles, and since the Stark energy shift of the NH_3 ground state in fields up to 12 V cm^{-1} is <0.001 cm^{-1}, it was neglected. Under these conditions, in zero electric field the calculated resonance energy transfer cross section for $n = 40$ is $\sim 2 \times 10^{-11}$ cm^2. Assuming a pseudo-first-order kinetic model, this corresponds, under the experimental conditions, to an energy-transfer rate of $\sim 10^4$ s^{-1}, or a zero-field transition probability in 10-μs interaction time of $\sim$0.1. This is on the order of that observed in Figs. 3(c) and 3(d). The measured energy-transfer rates depend on the Boltzmann factors $P_{J,K}(T)$ reflecting the relative population of each $|J,K\rangle$ state [33]. These quantities and the wave numbers of the inversion transitions were calculated using the rotational constants $B = 9.44$ cm^{-1} and $C = 6.20$ cm^{-1} [33,35]. The products of $P_{J,K}(T)$ and $\mu_{J,K}$, i.e., the contribution from each $|J,K\rangle$ state to the energy-transfer rate, are displayed in Fig. 1(b).

The measured $|np\rangle$-electron signal associated with the energy-transfer process from each $|J,K\rangle$ state is proportional to $P_{J,K}(T)\,\sigma_{J,K}(F_{\rm int})$ and dependent upon the detuning from resonance. Assuming a Gaussian form with a FWHM of $\Delta E_{\rm FWHM}/hc \propto 1/\sqrt{\sigma_{J,K}(F_{\rm int})}$ for the dependence on the detuning [8], the solid curves in Fig. 4 were obtained with one global fit parameter: the constant of proportionality associated with the resonance width. This was found to be 18 D cm^{-1}, resulting in typical atom-molecule interaction times, e.g., at $n = 40$ in zero electric field, of 0.2 ns and hence resonance widths of $\Delta E_{\rm FWHM}/hc \simeq 0.17$ cm^{-1} ($\Delta E_{\rm FWHM}/h \simeq 5$ GHz).

The results of the calculations displayed in Fig. 4 account for the equal periods of 5 μs that the atoms spend in zero electric field and in $F_{\rm int}$ and are in good agreement with the measured dependence of the energy-transfer process on $F_{\rm int}$. It is noticeable that the fields for which maximal energy transfer is observed at each value of n are lower than those for which the Rydberg-Rydberg transition wave number coincides exactly with the centroid of the NH_3 inversion spectrum (dashed vertical lines in Fig. 4). This shift arises from the dependence of $\mu_{ns',np'}(F_{\rm int})$ on $F_{\rm int}$. For each value of n, $\mu_{ns',np'}(F_{\rm int})$ is maximal when $F_{\rm int} = 0$ V cm^{-1}. As the $|ns\rangle$ and $|np\rangle$ states mix in the field, $\mu_{ns',np'}(F_{\rm int})$ decreases. Consequently, for each value of n, the dipole-dipole coupling between the collision partners is largest in electric fields below those that satisfy the resonance condition and falls off as the field is tuned through resonance. For the higher values of n [Figs. 4(d)–4(f)], the measured population transfer to the $|np\rangle$ states is lower than expected when compared to the observations at $n = 36$. This may be a result of additional energy-transfer channels opening as the value of n increases [20] or an effect of individual atoms undergoing multiple collisions, with a small contribution from the n dependence of the Rydberg state fluorescence lifetimes, which range from 36 μs (56 μs) to 53 μs (83 μs) for the $|36s\rangle$ ($|36p\rangle$) to $|41s\rangle$ ($|41p\rangle$) states in zero field.

V. CONCLUSION

The studies of the effects of electric fields on Förster resonance energy transfer between NH_3 and Rydberg He atoms reported here open opportunities for investigations of the contributions of collision energy, particle orientation, and coherence in the energy-transfer process. By using beams of strongly interacting Rydberg atoms with large static electric dipole moments [30], it will be possible to investigate many-body effects in carefully controlled environments. To achieve maximal control over the collisional partners it will be desirable to employ guided or decelerated molecular beams [36–38]. These techniques, combined with the methods of Rydberg-Stark deceleration [39], are well suited to low-energy collision experiments [40,41].

Note added in proof. Recently, it has been suggested that resonant energy transfer between polar ground state molecules and Rydberg atoms could be exploited for non-destructive detection of cold molecules [42].

ACKNOWLEDGMENTS

This work is supported by the Engineering and Physical Sciences Research Council under Grant No. EP/L019620/1 and the European Research Council (ERC) under the European Union's Horizon 2020 research and innovation program (Grant Agreement No. 683341).

[1] D. L. Andrews and A. A. Demidov, *Resonance Energy Transfer* (Wiley, London, 1999).
[2] G. D. Scholes, Long-range resonance energy transfer in molecular systems, Annu. Rev. Phys. Chem. **54**, 57 (2003).
[3] J. Perrin, Fluorescence et induction moléculaire par résonance, C. R. Acad. Sci. **184**, 1097 (1927).
[4] T. Förster, Energiewanderung und Fluoreszenz, Naturwissenschaften **33**, 166 (1946).
[5] T. Förster, Zwischenmolekulare Energiewanderung und Fluoreszenz, Ann. Phys. (Berlin, Ger.) **437**, 55 (1948).
[6] T. Ha, T. Enderle, D. F. Ogletree, D. S. Chemla, P. R. Selvin, and S. Weiss, Probing the interaction between two single molecules: Fluorescence resonance energy transfer between a single donor and a single acceptor, Proc. Natl. Acad. Sci. USA **93**, 6264 (1996).
[7] Y.-C. Cheng and G. R. Fleming, Dynamics of light harvesting in photosynthesis, Annu. Rev. Phys. Chem. **60**, 241 (2009).
[8] T. F. Gallagher, Resonant collisional energy transfer between Rydberg atoms, Phys. Rep. **210**, 319 (1992).
[9] T. F. Gallagher and P. Pillet, Dipole-dipole interactions of Rydberg atoms, Adv. At. Mol. Opt. Phys. **56**, 161 (2008).
[10] B. G. Richards and R. R. Jones, Dipole-dipole resonance line shapes in a cold Rydberg gas, Phys. Rev. A **93**, 042505 (2016).
[11] E. A. Yakshina, D. B. Tretyakov, I. I. Beterov, V. M. Entin, C. Andreeva, A. Cinins, A. Markovski, Z. Iftikhar, A. Ekers, and I. I. Ryabtsev, Line shapes and time dynamics of the Förster resonances between two Rydberg atoms in a time-varying electric field, Phys. Rev. A **94**, 043417 (2016).
[12] W. Maineult, B. Pelle, R. Faoro, E. Arimondo, P. Pillet, and P. Cheinet, Dipole-quadrupole Förster resonance in cesium Rydberg gas, J. Phys. B **49**, 214001 (2016).
[13] T. Vogt, M. Viteau, J. Zhao, A. Chotia, D. Comparat, and P. Pillet, Dipole Blockade at Förster Resonances in High Resolution Laser Excitation of Rydberg States of Cesium Atoms, Phys. Rev. Lett. **97**, 083003 (2006).
[14] T. Wilk, A. Gaëtan, C. Evellin, J. Wolters, Y. Miroshnychenko, P. Grangier, and A. Browaeys, Entanglement of Two Individual Neutral Atoms Using Rydberg Blockade, Phys. Rev. Lett. **104**, 010502 (2010).
[15] O. Firstenberg, C. S. Adams, and S. Hofferberth, Nonlinear quantum optics mediated by Rydberg interactions, J. Phys. B **49**, 152003 (2016).
[16] D. Tiarks, S. Baur, K. Schneider, S. Dürr, and G. Rempe, Single-Photon Transistor Using a Förster Resonance, Phys. Rev. Lett. **113**, 053602 (2014).
[17] H. Gorniaczyk, C. Tresp, P. Bienias, A. Paris-Mandoki, W. Li, I. Mirgorodskiy, H. P. Büchler, I. Lesanovsky, and S. Hofferberth, Enhancement of Rydberg-mediated single-photon nonlinearities by electrically tuned Förster resonances, Nat. Commun. **7**, 12480 (2016).
[18] S. Ravets, H. Labuhn, D. Barredo, L. Béguin, T. Lahaye, and A. Browaeys, Coherent dipole-dipole coupling between two single Rydberg atoms at an electrically-tuned Förster resonance, Nat. Phys. **10**, 914 (2014).
[19] G. Günter, H. Schempp, M. Robert-de-Saint-Vincent, V. Gavryusev, S. Helmrich, C. S. Hofmann, S. Whitlock, and M. Weidemüller, Observing the dynamics of dipole-mediated energy transport by interaction-enhanced imaging, Science **342**, 954 (2013).
[20] K. A. Smith, F. G. Kellert, R. D. Rundel, F. B. Dunning, and R. F. Stebbings, Discrete Energy Transfer in Collisions of Xe(nf) Rydberg Atoms with NH_3 Molecules, Phys. Rev. Lett. **40**, 1362 (1978).
[21] L. Petitjean, F. Gounand, and P. R. Fournier, Depopulation of rubidium Rydberg states by CO molecules: An experimental and theoretical study, Phys. Rev. A **30**, 71 (1984).
[22] L. Petitjean, F. Gounand, and P. R. Fournier, Collisions of rubidium Rydberg-state atoms with ammonia, Phys. Rev. A **33**, 143 (1986).
[23] X. Ling, M. T. Frey, K. A. Smith, and F. B. Dunning, The role of inversion transitions in K(150p)/NH_3, ND_3 collisions, J. Chem. Phys. **98**, 2486 (1993).
[24] S. D. Huber and H. P. Büchler, Dipole-Interaction-Mediated Laser Cooling of Polar Molecules to Ultracold Temperatures, Phys. Rev. Lett. **108**, 193006 (2012).
[25] B. Zhao, A. W. Glaetzle, G. Pupillo, and P. Zoller, Atomic Rydberg Reservoirs for Polar Molecules, Phys. Rev. Lett. **108**, 193007 (2012).
[26] G. D. Scholes, Quantum-coherent electronic energy transfer: Did Nature think of it first?, J. Phys. Chem. Lett. **1**, 2 (2010).
[27] A. Chenu and G. D. Scholes, Coherence in energy transfer and photosynthesis, Annu. Rev. Phys. Chem. **66**, 69 (2015).
[28] J. Jankunas, K. Jachymski, M. Hapka, and Andreas Osterwalder, Observation of orbiting resonances in He($^3S_1$) + NH_3 Penning ionization, J. Chem. Phys. **142**, 164305 (2015).
[29] T. Halfmann, J. Koensgen, and K. Bergmann, A source for a high-intensity pulsed beam of metastable helium atoms, Meas. Sci. Technol. **11**, 1510 (2000).
[30] V. Zhelyazkova, R. Jirschik, and S. D. Hogan, Mean-field energy-level shifts and dielectric properties of strongly polarized Rydberg gases, Phys. Rev. A **94**, 053418 (2016).
[31] G. Scholes, *Atomic and Molecular Beam Methods* (Oxford University Press, New York, 1988), Vol. 1.
[32] G. W. F. Drake, High precision theory of atomic helium, Phys. Scr. **T83**, 83 (1999).
[33] C. H. Townes and A. L. Schawlow, *Microwave Spectroscopy* (McGraw-Hill, London, 1955).
[34] M. L. Zimmerman, M. G. Littman, M. M. Kash, and D. Kleppner, Stark structure of the Rydberg states of alkali-metal atoms, Phys. Rev. A **20**, 2251 (1979).
[35] C. C. Costain, An empirical formula for the microwave spectrum of ammonia, Phys. Rev. **82**, 108 (1951).
[36] H. L. Bethlem, G. Berden, and G. Meijer, Decelerating Neutral Dipolar Molecules, Phys. Rev. Lett. **83**, 1558 (1999).

[37] S. Y. T. van de Meerakker, H. L. Bethlem, N. Vanhaecke, and G. Meijer, Manipulation and control of molecular beams, Chem. Rev. **112**, 4828 (2012).

[38] J. Jankunas and A. Osterwalder, Cold and controlled molecular beams: Production and applications, Annu. Rev. Phys. Chem. **66**, 241 (2015).

[39] S. D. Hogan, Rydberg-Stark deceleration of atoms and molecules, EPJ Tech. Instrum. **3**, 1 (2016).

[40] J. Onvlee, S. D. S. Gordon, S. N. Vogels, T. Auth, T. Karman, B. Nichols, A. van der Avoird, G. C. Groenenboom, M. Brouard, and S. Y. T. van de Meerakker, Imaging quantum stereodynamics through Fraunhofer scattering of NO radicals with rare-gas atoms, Nat. Chem. **9**, 226 (2017).

[41] P. Allmendinger, J. Deiglmayr, O. Schullian, K. Höveler, J. A. Agner, H. Schmutz, and F. Merkt, New method to study ion-molecule reactions at low temperatures and application to the $H_2^+ + H_2 \rightarrow H_3^+ + H$ reaction, ChemPhysChem **17**, 3596 (2016).

[42] M. Zeppenfeld, Nondestructive detection of polar molecules via Rydberg atoms, arXiv:1611.08893 (2016).